Comprehensive constraints on heavy sterile neutrinos from core-collapse supernovae

Pierluca Carenza,[1,*] Giuseppe Lucente,[2,3,4,5,†] Leonardo Mastrototaro,[6,7,‡] Alessandro Mirizzi,[2,3,§] and Pasquale Dario Serpico[8,‖]

[1]*The Oskar Klein Centre, Department of Physics, Stockholm University, Stockholm 106 91, Sweden*
[2]*Dipartimento Interateneo di Fisica "Michelangelo Merlin", Via Amendola 173, 70126 Bari, Italy*
[3]*Istituto Nazionale di Fisica Nucleare - Sezione di Bari, Via Orabona 4, 70126 Bari, Italy*
[4]*Institut für Theoretische Physik, Universität Heidelberg, Philosophenweg 16, 69120, Heidelberg, Germany*
[5]*Universität Heidelberg, Kirchhoff-Institut für Physik, Im Neuenheimer Feld 227, 69120 Heidelberg, Germany*
[6]*Dipartimento di Fisica "E.R. Caianiello", Università degli Studi di Salerno, Via Giovanni Paolo II, 132–84084 Fisciano (SA), Italy*
[7]*INFN—ruppo Collegato di Salerno, Via Giovanni Paolo II, 132–84084 Fisciano (SA), Italy*
[8]*LAPTh, CNRS, USMB, F-74000 Annecy, France*

(Received 10 November 2023; accepted 14 February 2024; published 8 March 2024)

Sterile neutrinos with masses up to $\mathcal{O}(100)$ MeV can be copiously produced in a supernova (SN) core through the mixing with active neutrinos. In this regard, the SN 1987A detection of neutrino events has been used to put constraints on active-sterile neutrino mixing, exploiting the well-known SN cooling argument. We refine the calculation of this limit including neutral current interactions with nucleons, which constitute the dominant channel for sterile neutrino production. We also include, for the first time, the charged current interactions between sterile neutrinos and muons, relevant for the production of sterile neutrinos mixed with muon neutrinos in the SN core. Using the recent modified luminosity criterion, we extend the bounds to the case where sterile states are trapped in the stellar core. Additionally, we study the decays of heavy sterile neutrinos, affecting the SN explosion energy and possibly producing a gamma-ray signal. We also illustrate the complementarity of our new bounds with cosmological bounds and laboratory searches.

DOI: 10.1103/PhysRevD.109.063010

I. INTRODUCTION

In the last decade, new theoretical ideas to address dark matter and other fundamental questions predict a dark sector composed of feebly interacting particles (FIPs) with sub-GeV masses and very feeble interactions with Standard Model (SM) particles [1–4]. The most common approach to describe the interaction of the dark sector with the SM is through some *portal*. In this regard, the minimal portals mixing new dark sector states with gauge-invariant combinations of SM fields are vector (dark photons), scalar (dark Higgs), fermion (heavy neutral leptons), and pseudoscalar (axions) [1]. These portals are the subject of intense experimental investigations with interesting plans for the next years [1–4].

In this context, core-collapse supernovae (SNe) are recognized as a powerful laboratory not only to probe fundamental neutrino properties [5–7], but also the emission of FIPs (see, e.g., Refs. [3,4,8,9]). Indeed, for typical core temperatures $T \simeq \mathcal{O}(30)$ MeV, FIPs with masses up to $\mathcal{O}(100)$ MeV [4] can be abundantly produced in a SN core. Notably, the physics case of axions and axionlike particles [10–18], dark photons [19–21], and dark Higgs [22] has been widely studied.

In this paper, we will focus on another class of FIPs, namely heavy neutral leptons and in particular a heavy sterile neutrino, ν_4, mostly a flavor-sterile one (ν_s) with a (generally small) mixing with active neutrinos ν_α, $\alpha = e, \mu, \tau$. These states have been often introduced to explain the origin of neutrino masses [23–26]. We remark that although the sterile neutrino scale considered here is not heavy for

*pierluca.carenza@fysik.su.se
†giuseppe.lucente@ba.infn.it
‡lmastrototaro@unisa.it
§alessandro.mirizzi@ba.infn.it
‖serpico@lapth.cnrs.fr

particle physics standards, it is so if compared to the current bounds on the mass scale in the active neutrino sector, i.e., $m_\nu \lesssim 1$ eV. Therefore, we will use the adjective *heavy* in this sense.

It is certainly not surprising that heavy sterile neutrinos, with masses well above the keV range, might have a strong impact on the SN dynamics [27–41]. These particles, once produced in the hot SN core, escape from the star subtracting energy form the star. This energy-loss channel [42,43] might have a sizable impact on the duration of the neutrino burst. Requiring compatibility with the SN 1987A observation in Kamiokande-II (KII) [44,45] and Irvine-Michigan-Brookhaven (IMB) [46,47] experiments (see Refs. [48,49] for recent reanalyses of the SN 1987A neutrino signal) excludes a portion of the sterile neutrino parameter space.

This constraint has been recently reevaluated in the *free-streaming* regime in Ref. [38], considering *weakly mixed* sterile neutrinos that escape the SN without interacting with stellar matter. However, recent developments in SN simulations and new proposals to improve FIP constraints from SNe suggest that the heavy-sterile neutrino limits can be significantly strengthened. It is worth noting that recent works, as Ref. [38], have considered the scattering of active neutrinos as the dominant channel for sterile neutrino production, neglecting the neutral current interactions with nucleons. The latter channel was expected to be suppressed due to the Fermi-blocking associated with nucleon degeneracy in the SN core. Nevertheless, in the few cases where nucleon scattering was considered, as in the seminal papers [42,43], the corresponding bounds were stronger than the ones obtained, e.g., in Ref. [38]. However, since the treatment of these processes in Refs. [42,43] was cursory, it seems to us important to revisit and clarify this issue. Additionally, from recent SN simulations [50,51], it emerges that a population of muons is present in the core and neutrinos interact with them through charged current interactions. These interactions are especially relevant in enhancing the production of sterile neutrinos mixed with muon neutrinos, allowing for an improvement of the previous bounds.

Furthermore, it is possible to constrain the ν_4 parameter space by studying the energy deposited inside a SN via the electromagnetic decays of sterile neutrinos. This is relevant for massive sterile neutrinos, where various decay channels are possible. For example, the decay $\nu_4 \to \pi^0 \nu_\mu$ would deposit at least 135 MeV of energy inside the SN [32,40]. In this regard, it has been recently shown in Ref. [15] that in order not to exceed the explosion energy observed in low-energy SNe, strong constraints can be placed on energy deposition induced by FIP decays. This argument has been applied to the heavy sterile neutrino case in Ref. [52]. Finally, the flux of daughter particles produced outside the SN, especially e^+ and γ, may lead to strong bounds (see Ref. [53] for a seminal study on ν_4) similarly to the ones recently discussed in Refs. [17,54–58] for the case of heavy axionlike particles.

Given these motivations, we devote this work to strengthen the existing bounds on heavy sterile neutrinos from SNe exploring different aspects:

(i) Including neutral current interactions of ν_4 with nucleons;
(ii) Including charged current interactions of ν_4 with muons;
(iii) Characterizing the trapping regime of ν_4 verified at large mixing angles, adopting the so-called "modified luminosity criterion" (see Refs. [13,19,59]). This recently proposed recipe allows one to extend the SN energy-loss bounds also to the regime where ν_4 are strongly interacting with matter;
(iv) Considering (non)radiative decays of heavy neutrinos, we strengthen the cooling including the constraint from excessive energy deposition, following the method proposed in Ref. [15,52], and from an observable gamma-ray signal.

The plan for this paper is as follows. In Sec. II, we recall the heavy neutrino production in SNe and summarize the relevant production and absorption processes. Then in Sec. III, we discuss the different arguments presented in the literature to constrain FIPs from SNe, and we apply them to the case of heavy ν_4. In Sec. IV, we combine all our bounds and compare them with the other laboratory and cosmological constraints in the same mass range. We conclude in Sec. V. In Appendix, we discuss the details of the evaluation of the charged and neutral current interactions involving ν_4.

II. STERILE NEUTRINO PRODUCTION

We limit ourselves to heavy sterile neutrinos with masses 10 MeV $\lesssim m_4 \lesssim$ 600 MeV [60,61] to avoid any possible resonant production, which usually happens in the sub-MeV range [33,34,62]. In this mass range, since the mixing of a sterile neutrino with electron neutrino is very constrained (see, e.g., Ref. [3]), we assume that the sterile neutrino is mixed dominantly with one active neutrino ν_α, with $\alpha = \mu, \tau$, such as

$$\begin{aligned} \nu_\alpha &= U_{\alpha 1}\nu_\ell + U_{\alpha 4}\nu_4, \\ \nu_s &= -U_{\alpha 4}\nu_\ell + U_{s4}\nu_4, \end{aligned} \tag{2.1}$$

where ν_ℓ and ν_4 are a light and the heavy mass eigenstate, respectively, U is the unitary mixing matrix, linking mass and flavor states, and the most interesting parameter space corresponds to $|U_{\alpha 4}|^2 \ll 1$; i.e., ν_ℓ is mostly active and ν_4 is mostly sterile.

In the SN core, sterile neutrinos are produced via the processes listed in Table I. We characterize these processes closely following Ref. [38]. We have neglected the bremsstrahlung process $NN \to NN\nu\bar{\nu}$ since it is always subleading in the interesting parameter space. Indeed, as a production

TABLE I. Squared matrix elements for sterile neutrino scattering processes (assuming mixing with the species α, and $\beta \neq \alpha$), summed over initial and final states, where $\tilde{g}_L = -\frac{1}{2} + \sin^2\theta_W$, $g_R = \sin^2\theta_W$ [63]. The symmetry factor $S = 1/2!$ is already included when two identical particles are present in the same state (second row). The particles involved in each reaction are enumerated as $1 + 2 \leftrightarrow 3 + 4$. The last two processes are valid only in the case of mixing with the muon neutrino, $\alpha = \mu$. The terms $|\mathcal{M}|^2_{AA}$, $|\mathcal{M}|^2_{VA}$, and $|\mathcal{M}|^2_{VV}$ are reported in Appendix. In the $\mu N \leftrightarrow N'\nu_4$ matrix element, we neglected the terms of higher order in the nucleon momenta, thus working at leading order in a nonrelativistic approximation. Here, N and N' represent the different nucleons involved in the interaction in the initial and final states. Finally, for all the processes, we have considered their corresponding charged conjugate for the $\bar{\nu}_4$ production (the last two processes are irrelevant because of the absence of μ^+ in the SN core) and absorption.

Process	$\lvert U_{\alpha 4}\rvert^{-2}\lvert\mathcal{M}\rvert^2$
$\nu_\alpha + \bar{\nu}_\alpha \leftrightarrow \bar{\nu}_\alpha + \nu_4$	$64G_F^2(p_1\cdot p_3)(p_2\cdot p_4)$
$\nu_\alpha + \nu_\alpha \leftrightarrow \nu_\alpha + \nu_4$	$32G_F^2(p_1\cdot p_2)(p_3\cdot p_4)$
$\nu_\beta + \bar{\nu}_\beta \leftrightarrow \bar{\nu}_\alpha + \nu_4$	$16G_F^2(p_1\cdot p_3)(p_2\cdot p_4)$
$\nu_\alpha + \bar{\nu}_\beta \leftrightarrow \bar{\nu}_\beta + \nu_4$	$16G_F^2(p_1\cdot p_3)(p_2\cdot p_4)$
$\nu_\alpha + \nu_\beta \leftrightarrow \nu_\beta + \nu_4$	$16G_F^2(p_1\cdot p_2)(p_3\cdot p_4)$
$e^+ + e^- \leftrightarrow \bar{\nu}_\alpha + \nu_4$	$64G_F^2[\tilde{g}_L^2(p_1\cdot p_4)(p_2\cdot p_3) + g_R^2(p_1\cdot p_3)(p_2\cdot p_4) - \tilde{g}_L g_R m_e^2(p_3\cdot p_4)]$
$\nu_\alpha + e^- \leftrightarrow e^- + \nu_4$	$64G_F^2[\tilde{g}_L^2(p_1\cdot p_2)(p_3\cdot p_4) + g_R^2(p_1\cdot p_3)(p_2\cdot p_4) - \tilde{g}_L g_R m_e^2(p_1\cdot p_4)]$
$\nu_\alpha + e^+ \leftrightarrow e^+ + \nu_4$	$64G_F^2[g_L^2(p_1\cdot p_3)(p_2\cdot p_4) + \tilde{g}_R^2(p_1\cdot p_2)(p_3\cdot p_4) - \tilde{g}_L g_R m_e^2(p_1\cdot p_4)]$
$\nu_\alpha + N \leftrightarrow N + \nu_4$	$\lvert\mathcal{M}\rvert^2_{AA} + \lvert\mathcal{M}\rvert^2_{VA} + \lvert\mathcal{M}\rvert^2_{VV}$
$\mu^- + N \leftrightarrow N' + \nu_4$	$\lvert\mathcal{M}\rvert^2_{AA} + \lvert\mathcal{M}\rvert^2_{VA} + \lvert\mathcal{M}\rvert^2_{VV}$
$\mu^- + \nu_e \leftrightarrow e^- + \nu_4$	$64G_F^2(p_1\cdot p_2)(p_3\cdot p_4)$

channel, the computed luminosity according to the rate of [9] is inferior to the one associated to the other processes in Table I. As an absorption channel, it is suppressed compared to $N\nu \to N\nu$ for obvious phase-space reasons.

The production rate of sterile neutrinos per unit volume and energy can be written as

$$\frac{\mathrm{d}^2 n_4}{\mathrm{d}E_4 \mathrm{d}t} = \int \frac{\mathrm{d}^3 p_1}{(2\pi)^3 2E_1}\frac{\mathrm{d}^3 p_2}{(2\pi)^3 2E_2}\frac{\mathrm{d}^3 p_3}{(2\pi)^3 2E_3}\frac{4\pi E_4 p_4}{(2\pi)^3 2E_4} \times (2\pi)^4\delta^4(p_1+p_2-p_3-p_4)|\mathcal{M}|^2_{12\to 34} f_1 f_2 (1-f_3), \tag{2.2}$$

where E_4 and p_4 are energy and momentum of the sterile neutrino, f_i is the distribution function of ith particle involved in the process, and $|\mathcal{M}|^2_{12\leftrightarrow 34}$ is the sum of the squared amplitudes for collisional processes $1 + 2 \leftrightarrow 3 + 4$ relevant for the sterile production/absorption, reported in Table I. Given recent SN simulations including muons [50,51], here we consider for the first time reactions involving muons, also reported in Table I. Moreover, we also include the neutral current interaction between neutrinos and nuclei, which results to be one of the main channels for the production and absorption of the heavy state. Despite the fact that its possible relevance was already pointed out in Ref. [64], in most literature, it has been neglected, similarly to the process $\nu e^- \to \nu e^-$, due to the large assumed fermion degeneracy and Pauli blocking effect. The abundance and degeneracy of nucleons in the SN core can be assessed by considering that the nuclear medium is described in a relativistic mean-field (RMF) picture [65], according to which the nucleon distribution function f_N is given by [65]

$$f_N(p) = \frac{1}{1 + \exp\left[\left(\sqrt{p^2 + m_N^{*2}} - \mu_N^*\right)/T\right]}, \tag{2.3}$$

where $m_N^* = m_N + \Sigma_S$ is the effective nucleon mass, with Σ_S the so-called nuclear scalar self-energy, and μ_N^* the effective or kinetic chemical potential, defined as [65]

$$\mu_N^* = \mu_N - \Sigma_V, \tag{2.4}$$

where μ_N is the nucleon chemical potential including the nucleon rest mass, and Σ_V is the RMF vector self-energy. Thus, nucleons have Fermi-Dirac distribution functions equivalent to a noninteracting system with effective chemical potentials μ_N^* and particle masses m_N^*, and their degeneracy can be estimated by introducing the degeneracy parameter η_N defined as

$$\eta_N = \frac{\mu_N^* - m_N^*}{T}. \tag{2.5}$$

On the other hand, leptons in the SN simulations are described by the usual Fermi-Dirac distributions

$$f_l(p) = \frac{1}{1 + \exp\left[\left(\sqrt{p^2 + m_l^2} - \mu_l\right)/T\right]}, \tag{2.6}$$

with m_l their bare mass and μ_l their chemical potential, leading to the degeneracy parameter

$$\eta_l = \frac{\mu_l - m_l}{T}. \tag{2.7}$$

We mention here that electrons in the plasma acquire an effective mass that for typical SN conditions ($\mu_e \gg T \gg m_e$) can be written as $m_e^{*2} = e^2(\mu_e^2 + \pi^2 T^2)/8\pi^2$ [66]. This expression leads to $m_e^* \lesssim \mathcal{O}(10)$ MeV $\ll \mu_e$ in the SN core. Thus, using m_e or m_e^* marginally affects the evaluation of η_e in Eq. (2.7) [67], and consistently with our benchmark SN model described in the following, we neglect m_e^* in our analysis. Particles i in the plasma are nondegenerate if $\eta_i < 0$, while they are fully degenerate for $\eta_i \gg 1$ and only partially degenerate for intermediate values of η_i [9].

We compute the sterile neutrino production using as a benchmark an $18M_\odot$ progenitor mass (roughly consistent with Sanduleak-69 202, the progenitor of the SN 1987A) obtained using a 1D spherically symmetric and general relativistic hydrodynamics model, based on the AGILE BOLTZTRAN code [68,69], including muons. While we expect that these simulations capture the basic physics of the phenomenon, differences of a factor of a few can be associated to the implementation scheme of the neutrino microphysics, general relativistic effects, multidimensionality, etc. We think that this constitutes the dominating systematic error in the derived bounds.

We show in Fig. 1 the thermodynamical conditions for our benchmark SN model in the inner core ($r \lesssim 20$ km) at the postbounce time $t_{\rm pb} = 1s$. The upper panel shows the temperature T (solid black line), with a peak $T \sim 40$ MeV at $r \sim 10$ km, and the matter density ρ (dashed black), with a maximum $\rho \sim 4 \times 10^{14}$ g cm^{-3} at the center and decreasing at larger radii. The central panel shows the fermion degeneracy parameters η_α for nucleons $\alpha = n,\ p$ and leptons $\alpha = e,\ \mu$. In the very inner core ($r \lesssim 5$ km), neutrons (solid black line) are degenerate ($\eta_n \approx 5$), and protons (dashed black line) are partially degenerate ($\eta_p \approx 2$). For larger radii ($r \gtrsim 10$ km), the nucleon degeneracy decreases, implying nondegenerate protons ($\eta_p < 0$) and only partially degenerate neutrons ($\eta_n \lesssim 1$). On the other hand, throughout the SN core, electrons (dotted black line) are highly degenerate ($\eta_e \gtrsim 5$) and muons (dot-dashed black line) are nondegenerate ($\eta_\mu < 0$). This implies that the $\nu e^- \to \nu e^-$ process is suppressed by the electron degeneracy, while neutral current interactions with nucleons cannot be neglected, at least in the outer layers of the core. Moreover, we checked that the conclusions concerning the η_e parameter are unchanged (with a discrepancy lower than 5%) even considering the effective electron mass due to QED at finite temperature and density, yielding $m_e^* \sim \mathcal{O}(10)$ MeV at $r \lesssim \mathcal{O}(10)$ km [66,67]. Finally, in the lower panel, we present the electron Y_e (solid line) and muon Y_μ (dashed line) abundance with respect to the nucleon one, with $Y_\alpha = n_\alpha/n_B$, where n_α is the density per unit volume for the particle $\alpha = e,\ \mu$, and n_B is the baryon number density. We realize that the muon abundance around the peak of the temperature can be $\mathcal{O}(10\%)$ of the nucleon one. Therefore, for definiteness, we evaluate the sterile neutrino production by taking into account also processes involving muons.

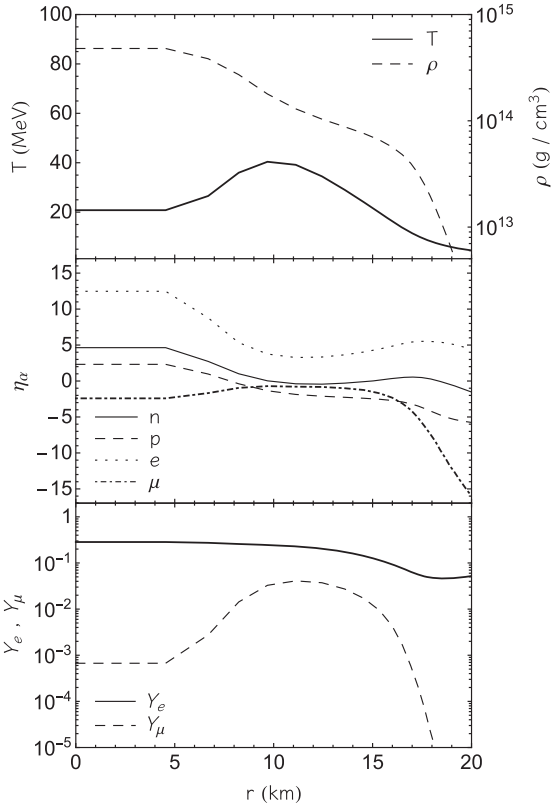

FIG. 1. *Upper panel*: Radial profiles of the temperature T (solid black line) and density ρ (dashed line) in the SN core. *Middle panel*: Radial profile for the degeneracy parameters of neutrons η_n (solid black line), protons η_p (dashed black), electrons η_e (dotted black), and muons η_μ (dot-dashed red). *Lower panel*: Radial profiles of the electron fraction Y_e (solid line) and muon fraction Y_μ (dashed line). All panels refer to the postbounce time $t_{\rm pb} = 1$ s.

We compute the production rate for sterile neutrinos by reducing the nine-dimensional integral in Eq. (2.2) to a three-dimensional one following the procedure in Ref. [70]. As an example, in Appendix, we show how it is possible to write the interaction matrix elements for the charged current process process $\mu N \leftrightarrow N\nu_4$ and the neutral current interaction $\nu_\alpha N \leftrightarrow N\nu_4$ using the formalism in Ref. [70]. The same procedure can be applied to evaluate the interaction matrix elements for the other processes we consider.

III. SN CONSTRAINTS ON HEAVY STERILE NEUTRINOS

A. Cooling bound

From the observation of the $\bar{\nu}_e$ neutrino burst from SN 1987A [44–47], it is possible to infer the temporal

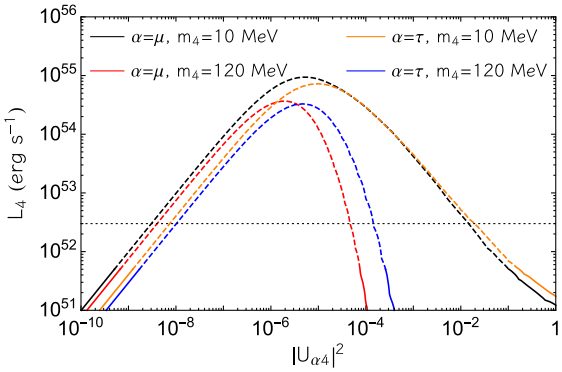

FIG. 2. Sterile neutrino luminosity as a function of $|U_{\alpha 4}|^2$ for $\alpha = \mu$, $m_4 = 10$ MeV and $m_4 = 120$ MeV (black and red lines, respectively) and the same for $\alpha = \tau$ (orange and blue lines, respectively). The horizontal dotted line corresponds to the limit value of $L_\nu = 3 \times 10^{52}$ erg s^{-1}. Dashed lines are used for values of the mixing where the sterile neutrino luminosity exceeds the luminosity of the species ν_α mixed with ν_4.

evolution of the neutrino light curve. Despite the sparseness of the data, the duration of the neutrino burst extending over 10 s is in agreement with the expectations from the SN cooling via neutrinos [9]. Therefore, from the SN 1987A neutrino data, there is no evidence of a dominant emission of FIPs that would have significantly shortened the duration of the neutrino burst [8,9].[1]

In order to avoid a significant shortening of the observed neutrino burst due to FIP emission, one should require that the luminosity of the exotic particles should be less then the one carried by neutrinos. Namely, for our fiducial model at $t_{\rm pb} = 1$ s, one has [8,9,59]

$$L_{\rm FIP} \lesssim L_\nu \equiv 3 \times 10^{52}\ {\rm erg\,s^{-1}}. \tag{3.1}$$

Our goal is to use this constraint to exclude values of the ν_4 mixing with muon neutrinos ($|U_{\mu 4}|^2$) and tau neutrinos ($|U_{\tau 4}|^2$). We do not consider the case of mixing with the electron flavor, since in this case, the parameter space is overconstrained. We adopt the "modified luminosity criterion" [13,19,59] to smoothly interpolate between the regimes in which sterile neutrinos are so weakly interacting that they freely escape from the SN (i.e., weak-mixing regime with $|U_{\alpha 4}|^2 \lesssim 10^{-5}$, see Fig. 2), also known as free-streaming regime, and a regime of stronger interactions with matter (i.e., strong-mixing regime with $|U_{\alpha 4}|^2 \gg 10^{-5}$, see Fig. 2), when they are trapped in analogy with active neutrinos. In this formalism, the ν_4 luminosity is [13,19,59,72]

$$L_4 = 4\pi \int_0^\infty {\rm d}r\, r^2\, \alpha^2(r) \int {\rm d}E_4 E_4 \frac{{\rm d}^2 n_4}{{\rm d}E_4 {\rm d}t} \langle e^{-\tau(E_4', r)} \rangle, \tag{3.2}$$

where α is the lapse factor to account for the gravitational redshift, and the exponential suppression $e^{-\tau}$ takes into account the possibility of ν_4 absorption inside the SN. In particular, $\langle e^{-\tau} \rangle$ is a directional average of the absorption factor [59,72–74]

$$\langle e^{-\tau(E',r)} \rangle = \frac{1}{2} \int_{-1}^{+1} {\rm d}\mu\, e^{-\int_0^\infty {\rm d}s\, \lambda^{-1}(E', \sqrt{r^2+s^2+2rs\mu})}, \tag{3.3}$$

where λ is the sterile neutrino mean-free path (mfp), $E' = E\alpha(r)/\alpha(\sqrt{r^2+s^2+2rs\mu})$ is the ν_4 redshifted energy, $\mu = \cos\beta$, and β is the angle between the outward radial direction and a given ray of propagation along which s is integrated. We emphasize that, lacking self-consistent SN simulations including the feedback due to the emission of sterile neutrinos, as the rest of the literature (implicitly) does, we also resort to an extrapolation whenever the extra neutrino luminosity is comparable with or larger than the luminosity of the species ν_α mixed with ν_4 (see dashed lines in Fig. 2). The results at values much larger than the active neutrino luminosity are, however, only nominal and not essential in obtaining the bound. Yet, it is conceivable that this limitation may introduce a factor of a few uncertainty in the limits from the cooling argument.

Sterile neutrinos with sufficiently strong interactions with ordinary matter are trapped in the SN via interactions with active neutrinos, electrons, positrons, and neutrons. The considered processes are listed in Table I. Moreover, depending on their mass, sterile neutrinos may decay in different particles after their production, through the processes shown in Table II. In Fig. 3, we show the branching ratios for the relevant decay channels. When evaluating the ν_4 absorption mfp, we have to consider absorptions and decays separately. In the former case, the mfp is defined as

$$\lambda_{\rm abs}^{-1}(E_4) = n\sigma(E_4), \tag{3.4}$$

where n is the density of targets, and σ is total absorption cross-section. Since all absorption processes in Table I are $2 \to 2$ scatterings, it is possible to write the following expression for the cross section:

$$\begin{aligned}\sigma(E_4) = \frac{1}{n}\frac{1}{2p_4} \int & \frac{{\rm d}^3p_1}{2E_1(2\pi)^3} \frac{{\rm d}^3p_2}{2E_2(2\pi)^3} \frac{{\rm d}^3p_3}{2E_3(2\pi)^3} \\ & \times (2\pi)^4 \delta^4(p_1 + p_2 - p_3 - p_4) |\mathcal{M}|^2 \\ & \times f_3(1-f_1)(1-f_2),\end{aligned} \tag{3.5}$$

with a suitable choice of Fermi-Dirac distribution functions f_i for $i = 1, 2, 3$, and of the matrix element $|\mathcal{M}|^2$, taken from Table I. In this context, the mfp can be explicitly evaluated by employing the procedure discussed in Ref. [70].

[1] In Ref. [49], it has been noticed that the latest three events of SN 1987A observed at $t_{\rm pb} \sim 10$ s are in tension with the state-of-the-art SN simulations. Inferring the luminosity bound only on the events observed by IMB up to $t_{\rm pb} \sim 5$ s, one expects a relaxation of the bound by a factor of 2 [71].

TABLE II. Decay channels up to $m_4 \lesssim 250$ MeV, for a ν_4 mixed with ν_μ where $f_\pi = 135$ MeV, $\tilde{g}_L = -\frac{1}{2} + \sin^2\theta_W$, $g_R = \sin^2\theta_W$, and the electron mass is neglected [38,75]. The decay mode into two muons is neglected since it is characterized by a small branching ratio for $m_4 < 500$ MeV, as shown in Fig. 3. The decay processes for the sterile neutrinos mixed with ν_τ via $|U_{\tau 4}|^2$ are the ones not involving a single muons in the final states, i.e., all but $\nu_4 \to \nu_e e^+ \mu^-$ and $\nu_4 \to \mu^- \pi^+$.

Process	$\Gamma/G_F^2 m_4^3 \lvert U_{\mu 4}\rvert^2$	Threshold (MeV)
$\nu_4 \to \nu_\mu \gamma$	$9\alpha m_4^2/2048\pi^4$	0
$\nu_4 \to \nu_\mu \nu_\mu \bar{\nu}_\mu$	$m_4^2/384\pi^3$	0
$\nu_4 \to \nu_\mu \nu_{e(\tau)} \bar{\nu}_{e(\tau)}$	$m_4^2/768\pi^3$	0
$\nu_4 \to \nu_\mu e^+ e^-$	$(\tilde{g}_L^2 + g_R^2) m_4^2/192\pi^3$	1.02
$\nu_4 \to \nu_e e^+ \mu^-$	$m_4^2/384\pi^3 (2(1 - m_\mu^2/m_4^2)(2 + 9m_\mu^2/m_4^2) + 2m_\mu^2/m_4 s^2(1 - m_\mu^2/m_4^2)$ $(-6 - 6m_\mu^2/m_4^2 + m_\mu^4/m_4^4 + 6\log m_\mu^2/m_4^2))$	106.2
$\nu_4 \to \nu_\mu \pi^0$	$f_\pi^2/32\pi(1 - m_\pi^2/m_4^2)^2$	139.6
$\nu_4 \to \nu_\mu \mu^+ \mu^-$	Neglected	211.2
$\nu_4 \to \mu^- \pi^+$	$\lvert V_{u\bar{d}}\rvert^2 f_\pi^2/32\pi((1 - m_\mu^2/m_4^2)^2 - m_\pi^2/m_4^2(1 + m_\mu^2/m_4^2))\sqrt{(1 - (m_\pi^2 + m_\mu^2)/m_4^2)^2 - 4m_\pi^2 m_\mu^2/m_4^4}$	245.3

Regarding the sterile neutrino decays, the mfp is defined as

$$\lambda_{\rm dec} = \frac{\gamma v}{\Gamma_{\rm tot}}, \tag{3.6}$$

where $\Gamma_{\rm tot}$ is the sum of the decay widths Γ of all the relevant decay processes (see Table II), $\gamma = (1 - \beta^2)^{-1/2}$ is the Lorentz factor, and the ν_4 velocity is $\beta = p/E_4$. Note that Dirac neutrinos are implicitly assumed throughout our paper; for Majorana states, the rates for exclusive processes are the same, but L-conjugated processes, e.g., in decays, are also allowed, thus doubling the inclusive rates.

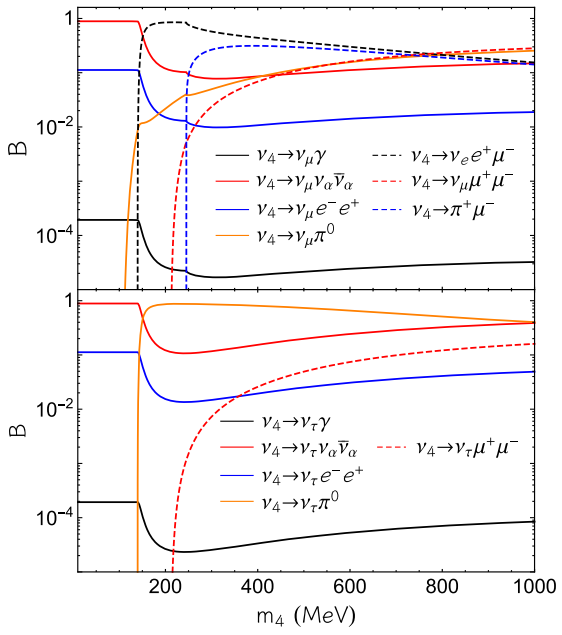

FIG. 3. Branching ratios for the relevant decay channels listed in Table II as a function of the sterile neutrino mass m_4 for a mixing with ν_μ (upper panel) and with ν_τ (lower panel).

By combining Eqs. (3.4) and (3.6), we obtain the total mfp as

$$\lambda^{-1} = \lambda_{\rm abs}^{-1} + \lambda_{\rm dec}^{-1}, \tag{3.7}$$

which is used to evaluate the sterile neutrino luminosity in Eq. (3.2) and impose the constraint in Eq. (3.1). Here, it is important to mention that for an unstable particle, the absorption factor in Eq. (3.3) would always be zero if the integration limit in the exponential were infinity (since unstable particles can decay in vacuum). However, it is possible to fix the upper integration limit in Eq. (3.3) to a far radius $R_{\rm far} = 100$ km [19,76,77], much larger than the protoneutron star radius $R_{\rm PNS} \approx 10$ km where sterile neutrinos are produced. This choice for $R_{\rm far}$ is an order-of-magnitude estimation for the neutrino gain radius [77]. In this way, we assume that only sterile neutrinos reaching the gain radius contribute to the SN cooling. Uncertainties related to the choice of $R_{\rm far}$ will not affect the conclusions of this work since the cooling bound is always subdominant with respect to other constraints, as discussed in the following.

The obtained bound is shown in Fig. 4. The contour area delimited by the solid line refers to the mixing with ν_μ, while the dashed line represents the bound for ν_τ mixing. This criterion excludes a region between $\mathcal{O}(10^{-9}) < |U_{\alpha 4}|^2 < \mathcal{O}(10^{-2})$ for $m_4 \sim \mathcal{O}(10)$ MeV, probing masses up to ~400 MeV for $|U_{\alpha 4}|^2 \sim \mathcal{O}(10^{-7})$. Our bound agrees at the order of magnitude level with the bound estimated in the seminal papers [42,43]. In the same figure, the dot-dashed black line shows the lower bound obtained neglecting the $\nu N \to N \nu_4$ interaction. Notice that this constraint is in agreement with the one obtained in Ref. [38] under the same assumption.[2] Thus, we confirm the crucial importance

[2]As a corollary, the magnitude of the signatures associated to benchmarks discussed in [38] remain roughly the same if the benchmark mixings adopted there are scaled down by the same amount as the tightening of the bounds in presence of neutral current interactions with nuclei.

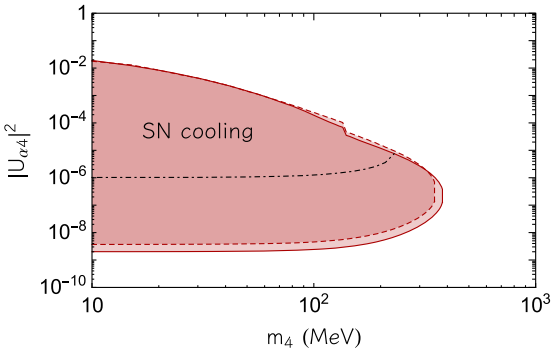

FIG. 4. Cooling bound on the sterile neutrino parameter space $(m_4, |U_{\alpha 4}|^2)$ for $\alpha = \mu$ (solid line) and $\alpha = \tau$ (dashed line). The dot-dashed black line is the bound for $|U_{\tau 4}|^2$ that would be obtained neglecting the $\nu N \to N\nu_4$ process as in Ref. [38].

of the inclusion of neutral interaction processes with nucleons in obtaining the lower exclusion bound on $|U_{\alpha 4}|^2$. Let us also highlight that the bound for $\alpha = \mu$ is a factor ~2 stronger than $\alpha = \tau$ because of the larger sterile neutrino luminosity caused by the presence of muons. Henceforth, bounds in the literature ignoring this effect tend to be too conservative. Note that in principle, following a calculation similar to the one in [38], a related bound might be obtained by the nonobservation of a high-energy neutrino flux, from sterile neutrino decay, in the experiments that detected the neutrino signal from the SN 1987A. Our estimates suggest that while comparable or slightly better than the cooling bound, this would not be competitive with other constraints discussed below and will not be considered further in this article.

B. SN explosion energy bound

As we can see from Table II, all the sterile neutrino decay channels except for $\nu_4 \to \nu_\mu \nu_\alpha \bar{\nu}_\alpha$ (with $\alpha = e, \mu, \tau$) produce photons, leptons, or pions. If sterile neutrinos have a decay length between the core radius of about 10 km and the progenitor star radius of about 10^{13} cm, they decay inside the SN envelope, depositing at least part of their energy inside the star. This phenomenon allows us to use SNe as efficient calorimeters. As proposed in Refs. [15,21], there is an upper limit on the amount of energy that can be deposited inside a SN by FIP decays without producing too energetic explosions that would be incompatible with observations of low-energy SNe. This constraint requires that

$$E_{\rm FIP}^{\rm e.m.} \lesssim 10^{50}\ {\rm erg}, \tag{3.8}$$

where $E_{\rm FIP}^{\rm e.m.}$ is the energy released in the electromagnetic sector by sterile neutrino decays.

In the decays, we assume that the daughter particles are emitted with an appropriate fraction of the energy in the center-of-mass frame, depending on the channel. Following Ref. [38], it is possible to write the deposited energy as

$$E_X^{\rm e.m.} = \sum_i B_i \frac{m_4}{2\bar{E}} \int {\rm d}t \int {\rm d}E E \int_{E_4^{\rm min}}^{\infty} {\rm d}E_4 \times \frac{1}{p_4} \frac{{\rm d}^2 N_4}{{\rm d}E_4 {\rm d}t} \left(1 - e^{-(R^* - R_{\rm p})/\lambda_{\rm dec}}\right), \tag{3.9}$$

where the index i runs over the decay processes under consideration, B_i is the branching ratio of the ith process, $\bar{E}$ and E are the daughter particle energies in the center-of-mass and in the laboratory frame, respectively, E_4 is the sterile neutrino energy, $R^* = 2.5 \times 10^{13}$ cm is the stellar radius, and [15,38]

$$E_4^{\rm min} = m_4 \frac{E^2 + \bar{E}^2}{2E\bar{E}},$$
$$\frac{{\rm d}^2 N_4}{{\rm d}E_4 {\rm d}t} = 4\pi \int_0^{R_{\rm p}} {\rm d}r\, r^2 \alpha^2(r) \frac{{\rm d}^2 n_4}{{\rm d}E_4 {\rm d}t} \langle e^{-\tau(E_4', r)} \rangle, \tag{3.10}$$

with ${\rm d}^2 N_4/{\rm d}E_4 {\rm d}t$ accounting for the fraction of sterile neutrinos escaping from the core, with $R_{\rm p} = 40$ km. In this way, we take into account only the energy carried out from the core and deposited by sterile neutrinos decaying in the SN envelope. We expect the bound in Eq. (3.8) to set a constraint on $|U_{\alpha 4}|^2$ 2 orders of magnitude more stringent than the SN cooling bound for sufficiently high ν_4 masses. At lower masses, the longer lifetime and larger boost factors imply that decays are not efficient, and this constraint is relaxed. Indeed, in Fig. 5, we see that for $m_4 > \mathcal{O}(100)$ MeV, the bound excludes values of the mixing down to $|U_{\alpha 4}|^2 \sim \mathcal{O}(10^{-10})$. The bump in the constraint around 135 MeV reflects the opening of an extra decay channel for sterile neutrinos, $\nu_4 \to \nu_\alpha \pi^0$. Recently, the authors of Ref. [52] have obtained a SN explosion energy bound without considering the $\nu N \to \nu_4 N$ interaction. Similarly to the SN cooling case, neglecting the neutral current interactions with nucleons leads to a constraint 2 orders of magnitude weaker than the one obtained in Fig. 5.

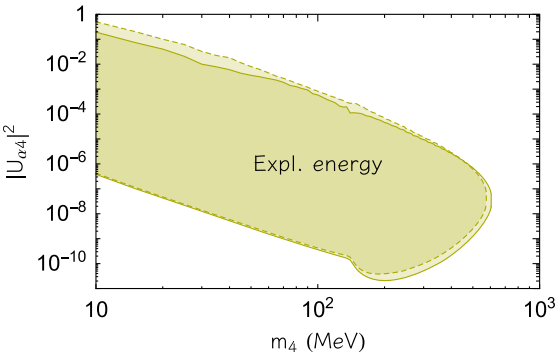

FIG. 5. Explosion energy bound on the sterile neutrino parameter space $(m_4, |U_{\alpha 4}|^2)$ for $\alpha = \mu$ (solid line) and $\alpha = \tau$ (dashed line).

C. 511 keV bound

Sterile neutrinos escaping the SN envelope and decaying in the interstellar medium give rise to a diverse phenomenology, depending on the considered decay products. Here, we focus on the positrons produced by a portion of the ν_4-decay channels.

As extensively discussed in Refs. [55,56,78,79], this exotic injection of positrons in the Galaxy would originate a distinctive soft gamma-ray signal. Precisely, positrons emitted by sterile neutrino decays are trapped in the Galaxy by its magnetic field. While traveling on scales smaller than $\mathcal{O}(1)$ kpc from the decay point, positrons lose energy by Bhabha scattering on the galactic electron population. This thermalization process lasts between 10^3 and 10^6 yrs, depending on the electron density. This long timescale explains why the positron injection, caused by SNe during the history of the Galaxy, can be assumed continuous. Once positrons are almost at rest, ∼25% of them form a parapositronium bound state with an electron, before decaying in two back-to-back photons, each one with an energy of 511 keV, determined by the electron rest mass [80].

A Galactic 511 keV line, at least partially explained by standard positron emission mechanisms, is prominently observed from the direction of the Galactic bulge [81]. The contribution to this signal induced by sterile neutrinos can be calculated as

$$\frac{\mathrm{d}\phi_\gamma^{511}}{\mathrm{d}\Omega} = 2k_{ps}N_{\mathrm{pos}}\Gamma_{cc}\int \mathrm{d}s\,\frac{n_{cc}[r(s,b,l),z(s,b)]}{4\pi}, \quad (3.11)$$

where $\mathrm{d}\Omega = \mathrm{d}l\,\mathrm{d}b\,\cos b$, with $-\pi \le l \le \pi$ being the longitude and $-\pi/2 \le b \le \pi/2$ being the latitude in the Galactic coordinate system (s,b,l), with s distance from the SN to the Sun. Moreover, $k_{ps} = 1/4$ accounts for the fraction of positrons annihilating through parapositronium. According to Ref. [82], we fix $\Gamma_{cc} = 2.30$ SNe/century as the Galactic SN rate. Finally, n_{cc} is the SN volume distribution [83] in the Galactocentric coordinate system (r,z,l), with r the galactocentric radius and z the height above the Galactic plane, connected with the Galactic coordinate system through the relations

$$r = \sqrt{s^2\cos^2 b + d_\odot^2 - 2d_\odot s\,\cos l\,\cos b},$$
$$z = s\,\sin b. \quad (3.12)$$

Here, we set the solar distance from the Galactic center to $d_\odot = 8.5$ kpc. Requiring the photon flux in Eq. (3.11) to be smaller than the observed signal in the range $l \in [28.25°; 31.25°]$ and $b \in [-10.75°; 10.25°]$, we obtain a constraint on the number of injected positrons [79]

$$N_{\mathrm{pos}} \lesssim 2.5 \times 10^{53}. \quad (3.13)$$

This is the most conservative limit obtained by the comprehensive analyses of Refs. [78,79], taking into account different SN distribution models and diffusive smearing effects. This upper bound on N_{pos} corresponds also to the constraint placed by XMM-Newton observations of the Galactic x-ray background [84]. Indeed, an excess of electron/positron injection in the Galaxy would source a diffuse x-ray signal via inverse Compton scattering on the stellar background light.

In order to apply the constraint in Eq. (3.13), we calculate the number of injected positrons as

$$N_{\mathrm{pos}} = n_{\mathrm{pos}}\int \mathrm{d}E_4\,\frac{\mathrm{d}N_4}{\mathrm{d}E_4}(\epsilon_{II}e^{-r_{II}/\lambda_{\mathrm{dec}}} + \epsilon_I e^{-r_I/\lambda_{\mathrm{dec}}}), \quad (3.14)$$

with

$$n_{\mathrm{pos}} = \sum_i n_i B_i, \quad (3.15)$$

the average number of positrons produced in a sterile neutrino decay. Moreover, following Ref. [20], we fix

$$r_{\mathrm{II}} = 10^{14}\ \mathrm{cm}, \qquad r_I = 2\times 10^{12}\ \mathrm{cm}, \quad (3.16)$$

for the envelope radii of Type II and Ib/c SNe, while according to Ref. [82], we take as average fractions of SNe of Type II and Ib/c

$$\epsilon_{II} = 1 - \epsilon_I, \qquad \epsilon_I = 0.33. \quad (3.17)$$

In Fig. 6, we show the calculated N_{pos} as a function of the mixing angle. At low mixing, sterile neutrinos are not efficiently produced, and, therefore, the number of positrons produced in the decay is smaller than the limiting value, represented by the dotted line. Then, as the sterile neutrino production increases, given that almost the totality of neutrinos decay inside the Galaxy, the injected positrons can be a sizable number. As it can be seen in Fig. 6, light sterile neutrinos with $m_4 = 20$ MeV (solid lines) can

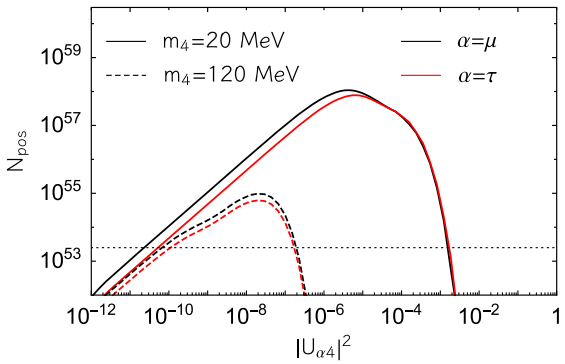

FIG. 6. Number of produced positrons per SN for $\alpha = \mu, \tau$ (black and red lines, respectively) and $m_4 = 20$ MeV (solid lines) and $m_4 = 120$ MeV (dashed lines). The dotted line corresponds to the limit value of $N_{\mathrm{pos}} = 2.5 \times 10^{53}$.

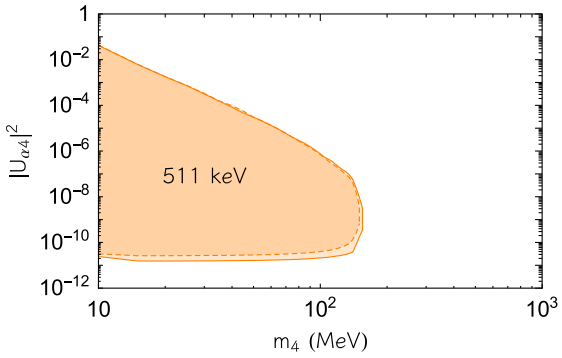

FIG. 7. 511 keV line bound on the sterile neutrino parameter space $(m_4, |U_{\alpha 4}|^2)$ for $\alpha = \mu$ (solid line) and $\alpha = \tau$ (dashed line).

produce up to $\sim 10^{58}$ positrons per SN. A smaller number is obtained by more massive neutrinos (dashed lines) since their production is Boltzmann suppressed. For small values of the mixing (e.g., $|U_{\alpha 4}|^2 \lesssim 10^{-6}$ for $m_4 = 20$ MeV), we notice a relatively small difference between sterile neutrinos mixed with muon neutrinos (black lines) or tau neutrinos (red lines) due to the larger production of the former ones induced by charged current interactions of muons with nucleons. For larger values of the mixing (e.g., $|U_{\alpha 4}|^2 \gtrsim 10^{-6}$ for $m_4 = 20$ MeV), the number of positrons is exponentially suppressed, and the different production and absorption processes lead to an even smaller difference in the positron production. The bound obtained with this approach is expected to exclude relatively light ν_4, with masses above a few tens of MeV, and it can be extended to small couplings because it is a cumulative diffuse flux. Indeed, we can see from Fig. 7 that the obtained lower bound is $|U_{\alpha 4}|^2 \sim \mathcal{O}(10^{-11})$ for $m_4 < \mathcal{O}(100)$ MeV.

D. SN 1987A gamma-ray bound

As discussed in the previous subsection, sterile neutrinos decaying after escaping the SN envelope lead to peculiar signatures. One of the most powerful constraints is given by the nondetection of a gamma-ray signal in coincidence with the neutrino burst of SN 1987A, as studied in the seminal work of Ref. [53]. The Gamma-Ray Spectrometer of the Solar Maximum Mission places an upper limit of [85]

$$\phi_\gamma \lesssim 1.38 \text{ cm}^{-2}, \tag{3.18}$$

on the photon flux at energies between 25 MeV and 100 MeV for 232.2 s after the first neutrino arrival. This upper limit translates into a constraint on $|U_{\alpha 4}|^2$ since the radiative decay of massive ν_4 would give rise to a gamma-ray signal in coincidence with a SN explosion. From Table II, we notice that the only decays contributing to this signal are $\nu_4 \to \nu_\alpha \gamma$ and $\nu_4 \to \nu_\alpha \pi^0$ because of the successive decay $\pi^0 \to \gamma\gamma$. The spectrum of photons originated by ν_4 decay directly into photons is [53]

$$\left(\frac{dN_\gamma}{dE_\gamma}\right)_{\text{dir}} = \frac{m_4}{2\bar{E}_{\nu_4 \to \nu_\alpha \gamma}} B_{\nu_4 \to \nu_\alpha \gamma} \int_{E^{\min}_{\nu_4 \to \nu_\alpha \gamma}}^{\infty} dE_4 \frac{1}{p_4} \frac{dN_4^{\text{esc}}}{dE_4}, \tag{3.19}$$

where the average energy, in the center-of-mass frame, of the daughter particle j, from the decay of the parent particle i is

$$\bar{E}_{i \to j} = \frac{m_i^2 - m_j^2}{2m_i}, \tag{3.20}$$

which is larger or equal to

$$E^{\min}_{i \to j} = m_i \frac{E_i^2 + \bar{E}_{i \to j}^2}{2E_i \bar{E}_{i \to j}}, \tag{3.21}$$

when expressed in the laboratory frame. In addition, the fraction of sterile neutrinos decaying outside the SN envelope is

$$\frac{dN_4^{\text{esc}}}{dE_4} = \frac{dN_4}{dE_4} e^{-R^*/\lambda_{\text{dec}}}. \tag{3.22}$$

Similarly to Eq. (3.19), we can evaluate the energy spectrum of neutral pions produced by sterile neutrinos as

$$\frac{dN_{\pi^0}}{dE_{\pi^0}} = \frac{m_4 B_{\nu_4 \to \nu_\alpha \pi^0}}{2\bar{E}_{\nu_4 \to \nu_\alpha \pi^0}} \int_{E^{\min}_{\nu_4 \to \nu_\alpha \pi^0}}^{\infty} \frac{dE_4}{p_4} \frac{dN_4^{\text{esc}}}{dE_4}. \tag{3.23}$$

In a second step, the gamma-ray spectrum from the almost immediate pion decay is obtained as [53]

$$\left(\frac{dN_\gamma}{dE_\gamma}\right)_{\pi^0} = \frac{m_{\pi^0}}{2\bar{E}_{\pi^0 \to \gamma\gamma}} \int_{E^{\min}_{\pi^0 \to \gamma\gamma}}^{\infty} \frac{dE_{\pi^0}}{p_{\pi^0}} \frac{dN_{\pi^0}}{dE_{\pi^0}}. \tag{3.24}$$

In conclusion, the expected gamma-ray flux can be written as

$$\frac{d\phi_\gamma}{dE_\gamma dt} = \frac{1}{4\pi d_{\text{SN}}^2} \frac{\beta e^{-t\beta/\lambda_{\text{dec}}}}{\lambda_{\text{dec}}} \frac{dN_\gamma}{dE_\gamma}, \tag{3.25}$$

where

$$\frac{dN_\gamma}{dE_\gamma} = \left(\frac{dN_\gamma}{dE_\gamma}\right)_{\text{dir}} + \left(\frac{dN_\gamma}{dE_\gamma}\right)_{\pi^0}. \tag{3.26}$$

We set stringent constraints on the sterile neutrino properties by integrating Eq. (3.25) over the observation time of 232.2 s and comparing the result with the limit in Eq. (3.18). The constraint obtained in this way becomes particularly relevant as soon as ν_4 is heavier than the pion, opening up the pion decay channel. Our results are reported in Fig. 8, showing that the lower bound strengthens from $|U_{\alpha 4}|^2 \gtrsim \mathcal{O}(10^{-10})$ for $m_4 < m_\pi$, m_π being the pion mass, to $|U_{\alpha 4}|^2 \gtrsim \mathcal{O}(10^{-12})$ for $m_4 > m_\pi$ due to the decay

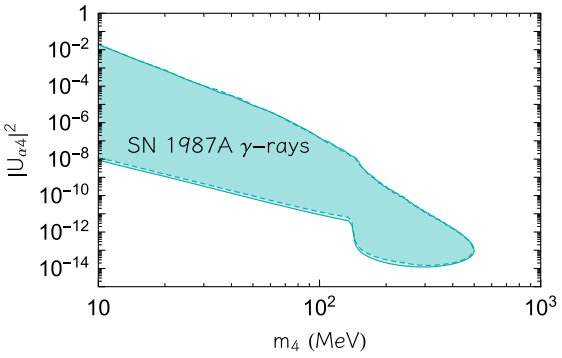

FIG. 8. Bound on the sterile neutrino parameter space $(m_4, |U_{\alpha 4}|^2)$ from the nondetection of gamma-rays from SN 1987A for $\alpha = \mu$ (solid line) and $\alpha = \tau$ (dashed line).

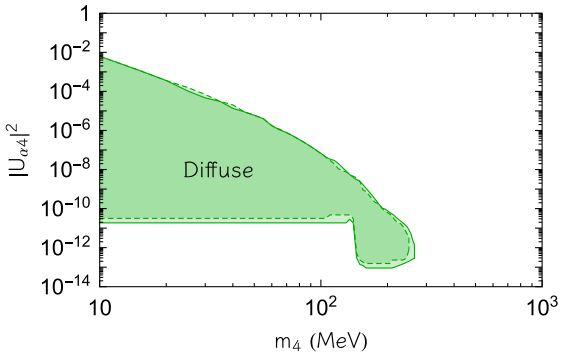

FIG. 9. Bound on the sterile neutrino parameter space $(m_4, |U_{\alpha 4}|^2)$ from diffuse gamma-ray emission for $\alpha = \mu$ (solid line) and $\alpha = \tau$ (dashed line).

channel $\nu_4 \to \nu_\alpha \pi$. As argued in [16] for axionlike particles, we mention that for sterile neutrinos with masses of a few 10 MeV, the decay-product photons may create a fireball, making part of the "SN 1987A gamma-rays" bound not valid. However, the fireball would produce a gamma-ray flux with energy of a few MeV, and the nondetection of such a signal in coincidence with the SN 1987A burst by Pioneer Venus Orbiter (PVO) constrains again this region, which, in turn, is already excluded by other bounds such as the 511 keV one.

E. Diffuse gamma-ray bound

The same phenomenology discussed above can be applied to evaluate the cumulative gamma-ray flux induced by SN ν_4 during the history of the Universe. This would constitute a diffuse, isotropic, and constant gamma-ray flux at a few tens of MeV.

The gamma-ray spectrum for a single SN is calculated as in Eq. (3.25), redshifted in energy and integrated over the SN explosion rate as (see Ref. [86] for calculation details in the case of the SN diffuse neutrino spectrum and Ref. [87] for the axion case)

$$\frac{\mathrm{d}\Phi_\gamma}{\mathrm{d}E_\gamma} = \int_0^\infty (1+z) \frac{\mathrm{d}N_\gamma(E_\gamma(1+z))}{\mathrm{d}E_\gamma} R_{\mathrm{SN}}(z) \left|\frac{\mathrm{d}t}{\mathrm{d}z}\right| \mathrm{d}z, \quad (3.27)$$

where z is the redshift, and $R_{\mathrm{SN}}(z)$ is the SN explosion rate taken from [88], with a total normalization for the core-collapse rate $R_{\mathrm{cc}} = 1.25 \times 10^{-4}\ \mathrm{yr}^{-1}\,\mathrm{Mpc}^{-3}$. Furthermore, $|\mathrm{d}t/\mathrm{d}z|^{-1} = H_0(1+z)[\Omega_\Lambda + \Omega_M(1+z)^3]^{1/2}$ with the cosmological parameters fixed at $H_0 = 67.4\ \mathrm{km\,s^{-1}\,Mpc^{-1}}$, $\Omega_M = 0.315$, $\Omega_\Lambda = 0.685$ [89]. The flux in Eq. (3.27) is imposed to be smaller than

$$\frac{\mathrm{d}\Phi_\gamma^{\mathrm{obs}}}{\mathrm{d}E_\gamma} = 2.2 \times 10^{-3} \left(\frac{E}{\mathrm{MeV}}\right)^{-2.2} \mathrm{MeV}^{-1}\,\mathrm{cm}^{-2}\,\mathrm{s}^{-1}\,\mathrm{sr}^{-1}, \quad (3.28)$$

extracted from measurements of Fermi-LAT of the diffuse gamma-ray background [54]. The advantage of this constraint, reported in Fig. 9, is that it extends to smaller masses, where the decay rate is less efficient, excluding $|U_{\mu 4}|^2 \gtrsim 2 \times 10^{-11}$ and $|U_{\tau 4}|^2 \gtrsim 3 \times 10^{-11}$ for $m_4 \lesssim 100$ MeV.

IV. COMBINATION OF DIFFERENT BOUNDS

In Fig. 10, we combine all the bounds obtained in the previous sections for ν_4 mixed with ν_μ (upper panel) and ν_τ (lower panel).

A. Laboratory bounds

Constraints on heavy sterile neutrinos decaying into leptons and pions are set by the long-baseline neutrino oscillation experiment T2K [97]. A beam of 30 GeV protons produced a large amount of kaons in their scattering on a graphite target at J-PARC. Then, kaons might produce sterile neutrinos in their decay. A detector placed at a baseline of 280 m was used to reveal the decay of sterile neutrinos. The constraints obtained by T2K complement and improve the results of CHARM [98] and PS191 [99]. Current experimental bounds are shown as the gray shaded area in Fig. 10.

The aforementioned searches will be improved by future experiments, whose projected sensitivities are shown as dashed lines in Fig. 10. In particular, current experimental constraints on sub-GeV sterile neutrinos considered in this work will be strengthened by DUNE [93,94], probing, however, regions not excluded by SN arguments only for masses $m_4 \gtrsim 400$ MeV, as shown by the dashed-black line in Fig. 10. Moreover, the future beam-dump experiment SHiP [3] is designed to probe exotic long-lived particles produced by a 400 GeV proton beam from the Super Proton Synchrotron at CERN, allowing the exploration of a much larger region of the parameter space for sterile neutrinos mixed with muon neutrinos [95], as represented by its sensitivity (dashed-red line) in the upper panel of Fig. 10. On the other hand, as shown by the dashed-brown line in

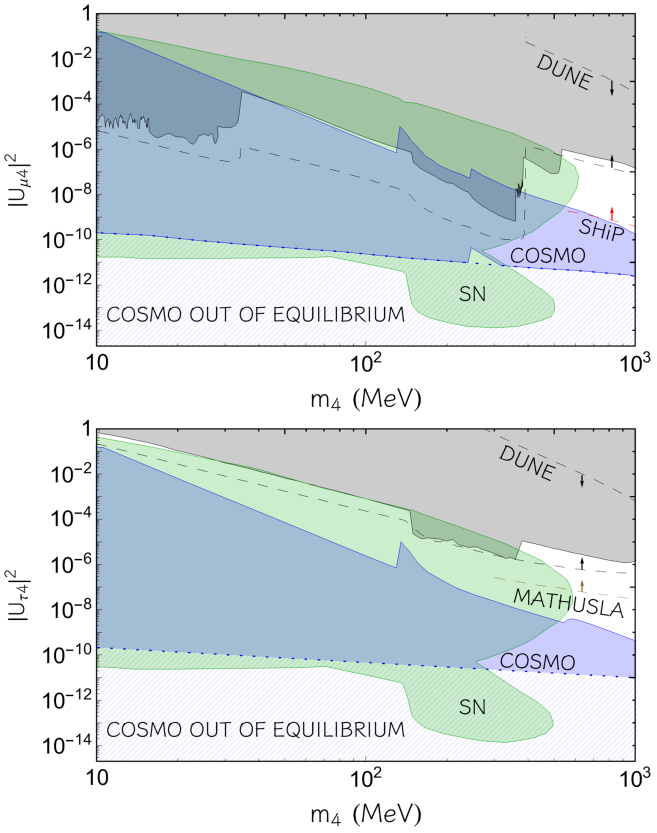

FIG. 10. Overview of the bounds from SNe (green region), cosmology [63,90,91] (blue region), and experiments [92] (gray region) for sterile neutrinos mixed with muon neutrinos (upper panel) and tau neutrinos (lower panel). The dashed lines represent the sensitivities of the future experiments DUNE [93,94] (black), SHiP [95] (red), and MATHUSLA [96] (brown). The hatched area below the dotted blue line represents the region of the parameter space in which sterile neutrinos are produced in the early Universe out of equilibrium, whose viability is more model dependent.

the lower panel of Fig. 10, a currently unexplored region of the parameter space of sterile neutrinos mixed with tau neutrinos will be probed by MATHUSLA [96], another CERN experiment planned to study sterile neutrinos by searching for displaced vertex signatures near the LHC interactions points.

B. Cosmological bound

Constraints on heavy sterile neutrinos from cosmological observations emerge considering that their decay, after the active neutrino decoupling, generates extra neutrino radiation and entropy production in the early Universe. Therefore, they alter the value of the effective number of neutrino species $N_{\rm eff}$, measured by the cosmic microwave background (CMB) and affect primordial nucleosynthesis (BBN), notably ^{4}He production, which is reflected in the Y_p value. Using the latest measurements of the Planck collaboration [89,100], it is possible to obtain cosmological constraints; see [63,90,91]. These arguments exclude up to $|U_{\alpha 4}|^2 \sim \mathcal{O}(10^{-1})$ for $m_4 \approx 10$ MeV, as represented by the blue region in Fig. 10 labeled as "COSMO." For heavier sterile neutrinos, with mass $m_4 > m_\pi$, the strongest impact on BBN is induced by the meson-driven $p \leftrightarrow n$ conversion, which significantly increases the helium abundance and constrains sterile neutrinos with lifetimes larger than 0.02 s [91]. The dotted blue line delimiting from below the blue region in Fig. 10 corresponds to the limit of validity of the assumptions used to obtain cosmological bounds. Indeed, these constraints are derived by considering only sterile neutrinos thermally produced and sufficiently short-lived so that they do not change the nuclear reaction framework by their meson decay products [91]. In this context, we mention that cosmological constraints may be extended also to the region of the parameter space in which sterile neutrinos are produced nonthermally (the hatched region below the dotted blue line, labeled as "COSMO OUT OF EQUILIBRIUM"), as discussed for instance in Ref. [101]. In this region, however, the bounds are more strongly dependent on the assumptions on the early Universe and the extra couplings of these states.

For ν_4 mixed with ν_μ, SN arguments lead to the lower limit $|U_{\mu 4}|^2 \gtrsim \mathcal{O}(10^{-11})$ for $m_a \lesssim 100$ MeV, notably due to the 511 keV line argument (see Sec. III C) and the diffuse gamma-ray flux (see Sec. III E). At larger masses, the SN bound tightens to $|U_{\mu 4}|^2 \lesssim 10^{-14}$ in the range 200 MeV $\lesssim m_4 \lesssim 500$ MeV due to the absence of gamma-rays in coincidence with SN 1987A (see Sec. III D). The existing laboratory bounds nicely complement the SN ones, excluding the parameter space all the way to large mixing angle and overlapping with SN bounds here dominated by the explosion energy argument (see Sec. III B). Future laboratory experiments are expected to charter new parameter space only for $m_4 \gtrsim 500$ MeV, probing mixing angles $10^{-6} \lesssim |U_{\mu 4}|^2 \lesssim 10^{-9}$. In the case of ν_4 mixed with ν_τ, the situation of the bounds is qualitatively similar. Factor $\sim$2 differences are due either to the extra production processes for sterile neutrinos associated with charged current interactions with muons or to the extra decay channels, present only for sterile neutrinos mixed with ν_μ.

V. CONCLUSIONS

In this work, we revised and improved current bounds on heavy sterile neutrinos mixed with the active ones. In particular, we considered the cooling bound derived from neutrino observations from SN 1987A. We also studied the decays of heavy sterile neutrinos, affecting the SN explosion energy and possibly producing a gamma-ray signal. We improved the characterization of sterile neutrino neutral current interactions of ν_4 with nucleons. We also include charged current interactions of ν_4 with muons, which is relevant for sterile neutrino production

mixing with ν_μ. Contrary to consolidate belief, it results that the dominant channel for sterile neutrino production is associated with neutral current interactions. Furthermore, we extended the bounds to the trapping regime of ν_4 verified at large mixing angles, adopting the so-called "modified luminosity criterion." We also strengthened the SN cooling bounds considering (non)radiative decays of heavy neutrinos and characterizing their effect on excessive energy deposition in the SN envelope and the observable gamma-ray signal when decays occur outside the SN. The combination of all the SN bounds (together with laboratory ones) allows one to exclude values $|U_{\alpha 4}|^2 \gtrsim 2$–$3 \times 10^{-11}$ for $m_a \lesssim 100$ MeV. At larger masses, the bound tightens to $|U_{\alpha 4}|^2 \lesssim 10^{-13}$–$10^{-14}$ in the range $200 \lesssim m_4 \lesssim 500$ MeV. It is worthwhile to mention that another possible astrophysical bound on sterile neutrinos comes from the observation of binary neutron star merger events (see, e.g., Ref. [102] for related constraints on axionlike particles). We reserve this analysis for future work. The most interesting region that SN bounds leave open for future laboratory searches (such as DUNE, SHiP, and MATHUSLA) is the range $10^{-6} \lesssim |U_{\mu 4}|^2 \lesssim 10^{-9}$ for $m_4 \gtrsim 500$ MeV. In the case of mixing with ν_τ, DUNE would also have the potential to robustly probe the range of masses down to $\sim$10 MeV at large mixings, where the overlap between SN and laboratory experiments is minimal or absent.

We conclude with two remarks. Having a synoptic view of the bounds following from SN arguments reveals that in most of the parameter space, at least a couple of arguments lead to constraints of similar strength. Since they suffer from different systematics, this is reassuring in supporting the overall reliability of such indirect limits. For instance, diffuse gamma-ray and 511 keV bounds rely on average properties of SN, such as their rate, rather than the single SN 1987A event. Also note that one does not have to rely on the cooling argument, which has been repeatedly criticized in recent years, to derive the strongest bounds from SN for heavy sterile neutrinos.

A similar remark applies on the relation between SN and cosmological bounds. It is reassuring that the bulk of the excluded parameter space overlaps. The underlying assumptions in deriving the two classes of bounds are indeed very different. For instance, in nonstandard cosmological scenarios with low-reheating temperatures, the BBN bounds can be lifted [103,104]. Since in astroparticle physics, one cannot control experimental conditions, the accumulation of independent ways to probe a certain type of new physics is essential for a broad acceptance of the robustness of the derived bounds.

ACKNOWLEDGMENTS

We warmly thank A. Lella for discussion during the preparation of this work. We are grateful to D. F. G. Fiorillo, M. Ovchynnikov, and E. Vitagliano for comments on the manuscript. P. C. and G. L. thank the Galileo Galilei Institute for Theoretical Physics for hospitality during the preparation of part of this work. This article is based upon work from COST Action COSMIC WISPers CA21106, supported by COST (European Cooperation in Science and Technology). The work of P. C. is supported by the European Research Council under Grant No. 742104 and by the Swedish Research Council (VR) under Grant Nos. 2018-03641 and 2019-02337. The work of L. M. is supported by the Italian Istituto Nazionale di Fisica Nucleare (INFN) through the "QGSKY" project and by Ministero dell'Università e Ricerca (MUR). The work of A. M. was partially supported by the research grant number 2022E2J4RK "PANTHEON: Perspectives in Astroparticle and Neutrino THEory with Old and New messengers" under the program PRIN 2022 funded by the Italian Ministero dell'Università e della Ricerca (MUR). G. L. is supported by the European Union's Horizon 2020 Europe research and innovation programme under the Marie Skłodowska-Curie Grant Agreement No. 860881-HIDDeN.

This work is (partially) supported by ICSC—Centro Nazionale di Ricerca in High Performance Computing, Big Data and Quantum Computing, funded by European Union—NextGenerationEU. The computational work has been executed on the IT resources of the ReCaS-Bari data center, which have been made available by two projects financed by the MIUR (Italian Ministry for Education, University and Re-search) in the "PON Ricerca e Competitività 2007-2013" Program: ReCaS (Azione I—Interventi di rafforzamento strutturale, PONa3_00052, Avviso 254/Ric) and PRISMA (Asse II—Sostegno all'innovazione, PON04a2A).

APPENDIX: PRODUCTION RATES FOR MASSIVE NEUTRINO PRODUCTION VIA NUCLEAR INTERACTIONS

Here, we discuss how to compute the production rates for the neutral current interactions with nucleons $\nu_\alpha(p_1) + N(p_2) \to N(p_3) + \nu_4(p_4)$ and the charged current process with muons $\mu(p_1) + N(p_2) \to N(p_3) + \nu_4(p_4)$.

In general, following the recipe in Ref. [70], the nine-dimensional integral for the production rate in Eq. (2.2) can be reduced to a three-dimensional integration that can be evaluated numerically. Explicitly,

$$\frac{\mathrm{d}^2 n_4}{\mathrm{d}E_4 \mathrm{d}t} = \frac{|U_{\alpha 4}|^2}{(2\pi)^6} p_4 \int_0^\infty \frac{p_3^2 \mathrm{d}p_3}{2E_3} \int_0^{p_3+p_4} \frac{p_1^2 \mathrm{d}p_1}{2E_1} \times \int \mathrm{d}\cos\theta\, M(p_1, p_3, p_4, \cos\theta) f_1 f_2 (1 - f_3), \tag{A1}$$

where $p_i = |\mathbf{p}_i|$, $\cos\theta = \mathbf{p}_1 \cdot \mathbf{p}_4 / p_1 p_4$, the integration limits for $\cos\theta$ are expressed in Ref. [70], and

$$M(p_1, p_3, p_4, \cos\theta) = \int dx |\mathcal{M}|^2 \tag{A2}$$

is an integral that can be analytically evaluated [70], with $x = \mathbf{p}_3 \cdot \mathbf{p}_4 / p_3 p_4$.

We compute the matrix elements for charged current processes $l^-(p_1) + N(p_2) \to N(p_3) + \nu_4(p_4)$ {see Eqs. (B1a)–(B1c) in Ref. [105]} without neglecting neither the charged lepton nor the neutrino mass, as usually done for the SM channels. In particular, we define $|\mathcal{M}|^2 = \langle|\mathcal{M}|^2\rangle_{VV} + \langle|\mathcal{M}|^2\rangle_{VA} + \langle|\mathcal{M}|^2\rangle_{AA}$, with

$$\langle|\mathcal{M}|^2\rangle_{VV} = 16\, G^2\, G_V^2 [(p_1 \cdot p_2)(p_3 \cdot p_4) + (p_2 \cdot p_4)(p_1 \cdot p_3) - m_2 m_3 (p_1 \cdot p_4)], \tag{A3}$$

$$\langle|\mathcal{M}|^2\rangle_{VA} = 32 G^2\, G_V\, G_A [(p_1 \cdot p_2)(p_3 \cdot p_4) - (p_2 \cdot p_4)(p_1 \cdot p_3)], \tag{A4}$$

$$\langle|\mathcal{M}|^2\rangle_{AA} = 16\, G^2\, G_A^2 [(p_1 \cdot p_2)(p_3 \cdot p_4) + (p_2 \cdot p_4)(p_1 \cdot p_3) + m_2 m_3 (p_1 \cdot p_4)]], \tag{A5}$$

$$G = G_F V_{\rm ud}, \tag{A6}$$

$$G_V = \frac{g_V \left(1 - \frac{q^2(\gamma_p - \gamma_n)}{4M_N^2}\right)}{\left(1 - \frac{q^2}{M_N^2}\right)\left(1 - \frac{q^2}{M_V^2}\right)^2}, \tag{A7}$$

$$G_A = \frac{g_A}{\left(1 - \frac{q^2}{M_A^2}\right)^2}. \tag{A8}$$

Here, G_F is the Fermi constant, $V_{\rm ud}$ is the up-down entry of the Cabibbo-Kobayashi-Maskawa matrix, γ_p and γ_n the magnetic moments of protons and neutrons, respectively, and $g_V = 1$ and $g_A = 1.27$ the vector and axial vector coupling constant, respectively. In addition, $M_V =$ 840 MeV is the vector mass, $M_A = 1$ GeV the axial mass, and M_N the nucleon mass, which, in the vacuum, is $M_N = 938$ MeV, while in the SN, plasma is reduced to an effective mass $M_N \sim \mathcal{O}(500)$ MeV due to nuclear self-interaction [65]. To numerically evaluate Eq. (A1), we have defined

$$\begin{aligned}
p_3 \cdot p_4 &= E_3 E_4 - p_3 p_4 x, \\
p_1 \cdot p_4 &= E_1 E_4 - p_1 p_4 \cos\theta, \\
p_2 \cdot p_4 &= m_4^2 + (E_3 E_4 - p_3 p_4 x) - (E_1 E_4 - p_1 p_4, \cos\theta), \\
p_1 \cdot p_3 &= (E_3 E_4 - p_3 p_4 x) - (E_1 E_4 - p_1 p_4 \cos\theta) + Q/2, \\
p_2 \cdot p_3 &= (E_1 E_4 - p_1 p_4 \cos\theta) + m_3^2 - Q/2, \\
p_1 \cdot p_2 &= (E_3 E_4 - p_3 p_4 x) - m_1^2 + Q/2, \\
Q &= m_1^2 + m_3^2 + m_4^2 - m_2^2.
\end{aligned}$$

With the above definition, we can write the three matrix element terms in Eqs. (A3)–(A5) as

$$\begin{aligned}
\langle|\mathcal{M}|^2\rangle_{VV} = {} & 8G^2\, G_V^2 [2\cos^2\theta p_1^2 p_4^2 + 2E_3 E_4 (2\cos\theta p_1 p_4 + m_4^2 - m_1^2 + Q) \\
& - E_1 E_4 (4\cos\theta p_1 p_4 + 2m_4^2 + 2m_2 m_3 + Q) + \cos\theta p_1\, p_4 (2\, m_4^2 + 2\, m_2\, m_3 + Q) \\
& + 2E_4^2 (2E_3^2 - 2E_1 E_3 + E_1^2) + m_4^2 Q] - 16G^2\, G_V^2 p_3 p_4 (2\cos\theta p_1 p_4 + 4E_3 E_4 - 2E_1 E_4 \\
& + m_4^2 - m_1^2 + Q)x + 32G^2 G_V^2 p_3^2 p_4^2 x^2,
\end{aligned} \tag{A9}$$

$$\begin{aligned}
\langle|\mathcal{M}|^2\rangle_{VA} = {} & 16 G_A G^2 G_V [-2E_3 E_4 (2\cos\theta p_1 p_4 + m_1^2 + m_4^2) + E_1 E_4 (4\cos\theta p_1 p_4 + 2m_4^2 + Q) \\
& - (\cos\theta p_1 p_4 + m_4^2)(2\cos\theta p_1 p_4 + Q) + 2E_4^2 E_1 (2E_3 - E_1)] \\
& + 32 G_A\, G^2\, G_V p_3 p_4\, (2\cos\theta p_1 p_4 - 2E_1 E_4 + m_1^2 + m_4^2)x,
\end{aligned} \tag{A10}$$

$$\begin{aligned}
\langle|\mathcal{M}|^2\rangle_{AA} = {} & 8G^2 G_A^2 [2\cos^2\theta p_1^2 p_4^2 + 2E_3 E_4 (2\cos\theta p_1 p_4 + m_4^2 - m_1^2 + Q) \\
& - E_1 E_4 (4\cos\theta p_1 p_4 + 2m_4^2 - 2m_2 m_3 + Q) + \cos\theta p_1 p_4 (2m_4^2 - 2m_2 m_3 + Q) \\
& + 2E_4^2 (2E_3^2 - 2E_1 E_3 + E_1^2) + m_4^2 Q] - 16G^2\, G_A^2 p_3 p_4 (2\cos\theta p_1 p_4 + 4E_3 E_4 - 2E_1 E_4 \\
& + m_4^2 - m_1^2 + Q)x + 32G^2 G_A^2 p_3^2 p_4^2 x^2.
\end{aligned} \tag{A11}$$

Finally, to obtain $M(p_1, p_3, p_4, \cos\theta)$ in Eq. (A1), we need to analytically integrate $|\mathcal{M}|^2$ over dx as shown in Eq. (A2) and discussed in Ref. [70].

The production rate for the neutral-current interaction $\nu_\alpha N \to N\nu_4$ can be computed in a way analogous to the charged-current one, with the replacements [106]

$$G_V \to G_V^n = \frac{1}{2}, \qquad G_V^p = \frac{1}{2} - 2\sin^2\theta_W, \tag{A12}$$

$$G_A \to G_A^n = \frac{g_A}{2}, \qquad G_A^p = \frac{g_A}{2}. \tag{A13}$$

These general expressions can be used to compute the emissivities for the processes $\nu_4 N \leftrightarrow \nu_\alpha N$ and $\nu_4 N \leftrightarrow \mu N$. On the other hand, details on the computation of the production rates for the other processes shown in Table I can be found in Ref. [38].

[1] G. Lanfranchi, M. Pospelov, and P. Schuster, The search for feebly interacting particles, Annu. Rev. Nucl. Part. Sci. **71**, 270 (2021).

[2] P. Agrawal *et al.*, Feebly-interacting particles: FIPs 2020 workshop report, Eur. Phys. J. C **81**, 1015 (2021).

[3] S. Alekhin *et al.*, A facility to search for hidden particles at the CERN SPS: The SHiP physics case, Rep. Prog. Phys. **79**, 124201 (2016).

[4] C. Antel *et al.*, Feebly interacting particles: FIPs 2022 workshop report, Eur. Phys. J. C **83**, 1122 (2023).

[5] A. Mirizzi, I. Tamborra, H.-T. Janka, N. Saviano, K. Scholberg, R. Bollig, L. Hudepohl, and S. Chakraborty, Supernova neutrinos: Production, oscillations and detection, Riv. Nuovo Cimento **39**, 1 (2016).

[6] H.-T. Janka, Explosion mechanisms of core-collapse supernovae, Annu. Rev. Nucl. Part. Sci. **62**, 407 (2012).

[7] H. T. Janka, Neutrino-driven explosions, in *Handbook of Supernovae* (Springer, Cham, 2017), 10.1007/978-3-319-21846-5_109.

[8] G. G. Raffelt, Astrophysical methods to constrain axions and other novel particle phenomena, Phys. Rep. **198**, 1 (1990).

[9] G. G. Raffelt, Stars as Laboratories for Fundamental Physics: The Astrophysics of Neutrinos, Axions, and Other Weakly Interacting Particles (The University of Chicago Press, 1996), https://press.uchicago.edu/ucp/books/book/chicago/S/bo3683609.html.

[10] P. Carenza, T. Fischer, M. Giannotti, G. Guo, G. Martínez-Pinedo, and A. Mirizzi, Improved axion emissivity from a supernova via nucleon-nucleon bremsstrahlung, J. Cosmol. Astropart. Phys. 10 (2019) 016; J. Cosmol. Astropart. Phys. 05 (2020) E01.

[11] P. Carenza, B. Fore, M. Giannotti, A. Mirizzi, and S. Reddy, Enhanced supernova axion emission and its implications, Phys. Rev. Lett. **126**, 071102 (2021).

[12] T. Fischer, P. Carenza, B. Fore, M. Giannotti, A. Mirizzi, and S. Reddy, Observable signatures of enhanced axion emission from protoneutron stars, Phys. Rev. D **104**, 103012 (2021).

[13] G. Lucente, P. Carenza, T. Fischer, M. Giannotti, and A. Mirizzi, Heavy axionlike particles and core-collapse supernovae: Constraints and impact on the explosion mechanism, J. Cosmol. Astropart. Phys. 12 (2020) 008.

[14] A. Caputo, P. Carenza, G. Lucente, E. Vitagliano, M. Giannotti, K. Kotake, T. Kuroda, and A. Mirizzi, Axionlike particles from hypernovae, Phys. Rev. Lett. **127**, 181102 (2021).

[15] A. Caputo, H.-T. Janka, G. Raffelt, and E. Vitagliano, Low-energy supernovae severely constrain radiative particle decays, Phys. Rev. Lett. **128**, 221103 (2022).

[16] M. Diamond, D. F. G. Fiorillo, G. Marques-Tavares, and E. Vitagliano, Axion-sourced fireballs from supernovae, Phys. Rev. D **107**, 103029 (2023); Phys. Rev. D **108**, 049902(E) (2023).

[17] A. Lella, P. Carenza, G. Lucente, M. Giannotti, and A. Mirizzi, Protoneutron stars as cosmic factories for massive axionlike particles, Phys. Rev. D **107**, 103017 (2023).

[18] A. Lella, P. Carenza, G. Co', G. Lucente, M. Giannotti, A. Mirizzi, and T. Rauscher, Getting the most on supernova axions, Phys. Rev. D **109**, 023001 (2024).

[19] J. H. Chang, R. Essig, and S. D. McDermott, Revisiting supernova 1987A constraints on dark photons, J. High Energy Phys. 01 (2017) 107.

[20] W. DeRocco, P. W. Graham, D. Kasen, G. Marques-Tavares, and S. Rajendran, Observable signatures of dark photons from supernovae, J. High Energy Phys. 02 (2019) 171.

[21] A. Sung, H. Tu, and M.-R. Wu, New constraint from supernova explosions on light particles beyond the Standard Model, Phys. Rev. D **99**, 121305 (2019).

[22] P. S. B. Dev, R. N. Mohapatra, and Y. Zhang, Revisiting supernova constraints on a light *CP*-even scalar, J. Cosmol. Astropart. Phys. 08 (2020) 003; J. Cosmol. Astropart. Phys. 11 (2020) E01.

[23] A. Merle, *Sterile Neutrino Dark Matter* (IOP Science Publishing, 2017), 10.1088/978-1-6817-4481-0.

[24] A. Boyarsky, M. Drewes, T. Lasserre, S. Mertens, and O. Ruchayskiy, Sterile neutrino dark matter, Prog. Part. Nucl. Phys. **104**, 1 (2019).

[25] K. N. Abazajian *et al.*, Light sterile neutrinos: A white paper, arXiv:1204.5379.

[26] K. N. Abazajian and A. Kusenko, Hidden treasures: Sterile neutrinos as dark matter with miraculous abundance, structure formation for different production mechanisms, and a solution to the σ_8 problem, Phys. Rev. D **100**, 103513 (2019).

[27] X. Shi and G. Sigl, A Type II supernovae constraint on electron-neutrino—sterile-neutrino mixing, Phys. Lett. B **323**, 360 (1994); Phys. Lett. B **324**, 516(E) (1994).
[28] H. Nunokawa, J. T. Peltoniemi, A. Rossi, and J. W. F. Valle, Supernova bounds on resonant active sterile neutrino conversions, Phys. Rev. D **56**, 1704 (1997).
[29] K. Abazajian, G. M. Fuller, and M. Patel, Sterile neutrino hot, warm, and cold dark matter, Phys. Rev. D **64**, 023501 (2001).
[30] J. Hidaka and G. M. Fuller, Dark matter sterile neutrinos in stellar collapse: Alteration of energy/lepton number transport and a mechanism for supernova explosion enhancement, Phys. Rev. D **74**, 125015 (2006).
[31] J. Hidaka and G. M. Fuller, Sterile Neutrino-enhanced supernova explosions, Phys. Rev. D **76**, 083516 (2007).
[32] G. M. Fuller, A. Kusenko, and K. Petraki, Heavy sterile neutrinos and supernova explosions, Phys. Lett. B **670**, 281 (2009).
[33] G. G. Raffelt and S. Zhou, Supernova bound on keV-mass sterile neutrinos reexamined, Phys. Rev. D **83**, 093014 (2011).
[34] C. A. Argüelles, V. Brdar, and J. Kopp, Production of keV sterile neutrinos in supernovae: New constraints and gamma ray observables, Phys. Rev. D **99**, 043012 (2019).
[35] A. M. Suliga, I. Tamborra, and M.-R. Wu, Tau lepton asymmetry by sterile neutrino emission—Moving beyond one-zone supernova models, J. Cosmol. Astropart. Phys. 12 (2019) 019.
[36] M. L. Warren, M. Meixner, G. Mathews, J. Hidaka, and T. Kajino, Sterile neutrino oscillations in core-collapse supernovae, Phys. Rev. D **90**, 103007 (2014).
[37] M. Warren, G. J. Mathews, M. Meixner, J. Hidaka, and T. Kajino, Impact of sterile neutrino dark matter on core-collapse supernovae, Int. J. Mod. Phys. A **31**, 1650137 (2016).
[38] L. Mastrototaro, A. Mirizzi, P. D. Serpico, and A. Esmaili, Heavy sterile neutrino emission in core-collapse supernovae: Constraints and signatures, J. Cosmol. Astropart. Phys. 01 (2020) 010.
[39] V. Syvolap, O. Ruchayskiy, and A. Boyarsky, Resonance production of keV sterile neutrinos in core-collapse supernovae and lepton number diffusion, Phys. Rev. D **106**, 015017 (2022).
[40] T. Rembiasz, M. Obergaulinger, M. Masip, M. A. Pérez-García, M.-A. Aloy, and C. Albertus, Heavy sterile neutrinos in stellar core-collapse, Phys. Rev. D **98**, 103010 (2018).
[41] A. Ray and Y.-Z. Qian, Evolution of tau-neutrino lepton number in protoneutron stars due to active-sterile neutrino mixing, Phys. Rev. D **108**, 063025 (2023).
[42] A. D. Dolgov, S. H. Hansen, G. Raffelt, and D. V. Semikoz, Cosmological and astrophysical bounds on a heavy sterile neutrino and the KARMEN anomaly, Nucl. Phys. **B580**, 331 (2000).
[43] A. D. Dolgov, S. H. Hansen, G. Raffelt, and D. V. Semikoz, Heavy sterile neutrinos: Bounds from big bang nucleosynthesis and SN1987A, Nucl. Phys. **B590**, 562 (2000).
[44] K. Hirata *et al.* (Kamiokande-II Collaboration), Observation of a neutrino burst from the supernova SN 1987a, Phys. Rev. Lett. **58**, 1490 (1987).
[45] K. S. Hirata *et al.*, Observation in the Kamiokande-II detector of the neutrino burst from supernova SN 1987a, Phys. Rev. D **38**, 448 (1988).
[46] R. M. Bionta *et al.*, Observation of a neutrino burst in coincidence with supernova SN 1987a in the large magellanic cloud, Phys. Rev. Lett. **58**, 1494 (1987).
[47] C. B. Bratton *et al.* (IMB Collaboration), Angular distribution of events from Sn1987a, Phys. Rev. D **37**, 3361 (1988).
[48] S. W. Li, J. F. Beacom, L. F. Roberts, and F. Capozzi, Old data, new forensics: The first second of SN 1987A neutrino emission, 2306.08024.
[49] D. F. G. Fiorillo, M. Heinlein, H.-T. Janka, G. Raffelt, E. Vitagliano, and R. Bollig, Supernova simulations confront SN 1987A neutrinos, Phys. Rev. D **108**, 083040 (2023).
[50] R. Bollig, H. T. Janka, A. Lohs, G. Martinez-Pinedo, C. J. Horowitz, and T. Melson, Muon creation in supernova matter facilitates neutrino-driven explosions, Phys. Rev. Lett. **119**, 242702 (2017).
[51] T. Fischer, G. Guo, G. Martínez-Pinedo, M. Liebendörfer, and A. Mezzacappa, Muonization of supernova matter, Phys. Rev. D **102**, 123001 (2020).
[52] G. Chauhan, S. Horiuchi, P. Huber, and I. M. Shoemaker, Low-energy supernovae bounds on sterile neutrinos, arXiv: 2309.05860.
[53] L. Oberauer, C. Hagner, G. Raffelt, and E. Rieger, Supernova bounds on neutrino radiative decays, Astropart. Phys. **1**, 377 (1993).
[54] F. Calore, P. Carenza, M. Giannotti, J. Jaeckel, and A. Mirizzi, Bounds on axionlike particles from the diffuse supernova flux, Phys. Rev. D **102**, 123005 (2020).
[55] F. Calore, P. Carenza, M. Giannotti, J. Jaeckel, G. Lucente, and A. Mirizzi, Supernova bounds on axionlike particles coupled with nucleons and electrons, Phys. Rev. D **104**, 043016 (2021).
[56] F. Calore, P. Carenza, M. Giannotti, J. Jaeckel, G. Lucente, L. Mastrototaro, and A. Mirizzi, 511 keV line constraints on feebly interacting particles from supernovae, Phys. Rev. D **105**, 063026 (2022).
[57] E. Müller, F. Calore, P. Carenza, C. Eckner, and M. C. D. Marsh, Investigating the gamma-ray burst from decaying MeV-scale axionlike particles produced in supernova explosions, J. Cosmol. Astropart. Phys. 07 (2023) 056.
[58] E. Ravensburg, P. Carenza, C. Eckner, and A. Goobar, Constraining MeV-scale axionlike particles with Fermi-LAT observations of SN 2023ixf, Phys. Rev. D **109**, 023018 (2024).
[59] A. Caputo, G. Raffelt, and E. Vitagliano, Muonic boson limits: Supernova redux, Phys. Rev. D **105**, 035022 (2022).
[60] T. Asaka, S. Blanchet, and M. Shaposhnikov, The nuMSM, dark matter and neutrino masses, Phys. Lett. B **631**, 151 (2005).
[61] T. Asaka and M. Shaposhnikov, The νMSM, dark matter and baryon asymmetry of the universe, Phys. Lett. B **620**, 17 (2005).
[62] A. M. Suliga, I. Tamborra, and M.-R. Wu, Lifting the core-collapse supernova bounds on keV-mass sterile neutrinos, J. Cosmol. Astropart. Phys. 08 (2020) 018.
[63] L. Mastrototaro, P. D. Serpico, A. Mirizzi, and N. Saviano, Massive sterile neutrinos in the early Universe: From

thermal decoupling to cosmological constraints, Phys. Rev. D **104**, 016026 (2021).
[64] G. Raffelt and G. Sigl, Neutrino flavor conversion in a supernova core, Astropart. Phys. **1**, 165 (1993).
[65] M. Hempel, Nucleon self-energies for supernova equations of state, Phys. Rev. C **91**, 055807 (2015).
[66] E. Braaten, Neutrino emissivity of an ultrarelativistic plasma from positron and plasmino annihilation, Astrophys. J. **392**, 70 (1992).
[67] G. Lucente and P. Carenza, Supernova bound on axionlike particles coupled with electrons, Phys. Rev. D **104**, 103007 (2021).
[68] A. Mezzacappa and S. W. Bruenn, A numerical method for solving the neutrino Boltzmann equation coupled to spherically symmetric stellar core collapse, Astrophys. J. **405**, 669 (1993).
[69] M. Liebendoerfer, O. E. B. Messer, A. Mezzacappa, S. W. Bruenn, C. Y. Cardall, and F. K. Thielemann, A finite difference representation of neutrino radiation hydrodynamics for spherically symmetric general relativistic supernova simulations, Astrophys. J. Suppl. Ser. **150**, 263 (2004).
[70] S. Hannestad and J. Madsen, Neutrino decoupling in the early universe, Phys. Rev. D **52**, 1764 (1995).
[71] G. Raffelt and D. Seckel, Bounds on exotic particle interactions from SN 1987a, Phys. Rev. Lett. **60**, 1793 (1988).
[72] A. Caputo, G. Raffelt, and E. Vitagliano, Radiative transfer in stars by feebly interacting bosons, J. Cosmol. Astropart. Phys. 08 (2022) 045.
[73] G. Lucente, L. Mastrototaro, P. Carenza, L. Di Luzio, M. Giannotti, and A. Mirizzi, Axion signatures from supernova explosions through the nucleon electric-dipole portal, Phys. Rev. D **105**, 123020 (2022).
[74] P. Carenza, Axion emission from supernovae: A cheat-sheet, Eur. Phys. J. Plus **138**, 836 (2023).
[75] D. Gorbunov and M. Shaposhnikov, How to find neutral leptons of the νMSM?, J. High Energy Phys. 10 (2007) 015; J. High Energy Phys. 11 (2013) 101(E).
[76] J. H. Chang, R. Essig, and S. D. McDermott, Supernova 1987A constraints on sub-GeV dark sectors, millicharged particles, the QCD axion, and an axionlike particle, J. High Energy Phys. 09 (2018) 051.
[77] H. A. Bethe, SN 1987A: An empirical and analytic approach, Astrophys. J. **412**, 192 (1993).
[78] P. De la Torre Luque, S. Balaji, and P. Carenza, Robust constraints on feebly interacting particles using XMM-Newton, arXiv:2307.13728.
[79] P. De la Torre Luque, S. Balaji, and P. Carenza, Multi-messenger search for electrophilic feebly interacting particles from supernovae, arXiv:2307.13731.
[80] S. G. Karshenboim, Precision study of positronium: Testing bound state QED theory, Int. J. Mod. Phys. A **19**, 3879 (2004).
[81] N. Prantzos *et al.*, The 511 keV emission from positron annihilation in the Galaxy, Rev. Mod. Phys. **83**, 1001 (2011).
[82] W. Li, R. Chornock, J. Leaman, A. V. Filippenko, D. Poznanski, X. Wang, M. Ganeshalingam, and F. Mannucci, Nearby supernova rates from the lick observatory supernova search. III. The rate-size relation, and the rates as a function of galaxy hubble type and colour, Mon. Not. R. Astron. Soc. **412**, 1473 (2011).
[83] A. Mirizzi, G. G. Raffelt, and P. D. Serpico, Earth matter effects in supernova neutrinos: Optimal detector locations, J. Cosmol. Astropart. Phys. 05 (2006) 012.
[84] J. W. Foster, M. Kongsore, C. Dessert, Y. Park, N. L. Rodd, K. Cranmer, and B. R. Safdi, Deep search for decaying dark matter with XMM-Newton blank-sky observations, Phys. Rev. Lett. **127**, 051101 (2021).
[85] L. Oberauer, C. Hagner, G. Raffelt, and E. Rieger, Supernova bounds on neutrino radiative decays, Astropart. Phys. **1**, 377 (1993).
[86] J. F. Beacom, The diffuse supernova neutrino background, Annu. Rev. Nucl. Part. Sci. **60**, 439 (2010).
[87] F. Calore, P. Carenza, C. Eckner, T. Fischer, M. Giannotti, J. Jaeckel, K. Kotake, T. Kuroda, A. Mirizzi, and F. Sivo, 3D template-based Fermi-LAT constraints on the diffuse supernova axionlike particle background, Phys. Rev. D **105**, 063028 (2022).
[88] A. Priya and C. Lunardini, Diffuse neutrinos from luminous and dark supernovae: Prospects for upcoming detectors at the $O(10)$ kt scale, J. Cosmol. Astropart. Phys. 11 (2017) 031.
[89] N. Aghanim *et al.* (Planck Collaboration), Planck 2018 results. VI. Cosmological parameters, Astron. Astrophys. **641**, A6 (2020); Astron. Astrophys. **652**, C4(E) (2021).
[90] N. Sabti, A. Magalich, and A. Filimonova, An extended analysis of heavy neutral leptons during big bang nucleosynthesis, J. Cosmol. Astropart. Phys. 11 (2020) 056.
[91] A. Boyarsky, M. Ovchynnikov, O. Ruchayskiy, and V. Syvolap, Improved big bang nucleosynthesis constraints on heavy neutral leptons, Phys. Rev. D **104**, 023517 (2021).
[92] P. D. Bolton, F. F. Deppisch, and P. S. Bhupal Dev, Neutrinoless double beta decay versus other probes of heavy sterile neutrinos, J. High Energy Phys. 03 (2020) 170.
[93] P. Ballett, T. Boschi, and S. Pascoli, Heavy neutral leptons from low-scale seesaws at the DUNE near detector, J. High Energy Phys. 03 (2020) 111.
[94] I. Krasnov, DUNE prospects in the search for sterile neutrinos, Phys. Rev. D **100**, 075023 (2019).
[95] C. Ahdida *et al.* (SHiP Collaboration), Sensitivity of the SHiP experiment to heavy neutral leptons, J. High Energy Phys. 04 (2019) 077.
[96] J. P. Chou, D. Curtin, and H. J. Lubatti, New detectors to explore the lifetime frontier, Phys. Lett. B **767**, 29 (2017).
[97] K. Abe *et al.* (T2K Collaboration), Search for heavy neutrinos with the T2K near detector ND280, Phys. Rev. D **100**, 052006 (2019).
[98] P. Vilain *et al.* (CHARM II Collaboration), Search for heavy isosinglet neutrinos, Phys. Lett. B **343**, 453 (1995).
[99] G. Bernardi *et al.*, Further limits on heavy neutrino couplings, Phys. Lett. B **203**, 332 (1988).
[100] M. Tanabashi *et al.* (Particle Data Group), Review of particle physics, Phys. Rev. D **98**, 030001 (2018).
[101] M. Ovchynnikov, Searches for new physics in the laboratory and in space, Ph.D. thesis, Leiden University, 2021.
[102] M. Diamond, D. F. G. Fiorillo, G. Marques-Tavares, I. Tamborra, and E. Vitagliano, Multimessenger constraints

on radiatively decaying axions from GW170817, arXiv: 2305.10327.

[103] G. Gelmini, S. Palomares-Ruiz, and S. Pascoli, Low reheating temperature and the visible sterile neutrino, Phys. Rev. Lett. **93**, 081302 (2004).

[104] G. Gelmini, E. Osoba, S. Palomares-Ruiz, and S. Pascoli, MeV sterile neutrinos in low reheating temperature cosmological scenarios, J. Cosmol. Astropart. Phys. 10 (2008) 029.

[105] G. Guo, G. Martínez-Pinedo, A. Lohs, and T. Fischer, Charged-current muonic reactions in core-collapse supernovae, Phys. Rev. D **102**, 023037 (2020).

[106] S. W. Bruenn, Stellar core collapse: Numerical model and infall epoch, Astrophys. J. Suppl. Ser. **58**, 771 (1985).